



Carbon dioxide gas sensing behavior of nanostructured GdCoO₃ prepared by a solution-polymerization method

Carlos R. Michel*, Alma H. Martínez, Fátima Huerta-Villalpando, Juan P. Morán-Lázaro

Departamento de Física, CUCEI, Universidad de Guadalajara, Marcelino García Barragán 1421, Guadalajara, Jalisco 44410, Mexico

ARTICLE INFO

Article history:

Received 23 January 2009

Received in revised form 10 April 2009

Accepted 1 May 2009

Available online 9 May 2009

Keywords:

Nanostructures

Chemical synthesis

Electrical characterization

Gas sensors

ABSTRACT

In this work, nanostructured GdCoO₃ powders were prepared by an aqueous solution-polymerization method using cobalt and gadolinium nitrates, and a mixture of polyvinyl alcohol and polyvinyl pyrrolidone. By X-ray powder diffraction GdCoO₃ was obtained at 650 °C in air. The microstructure of the powders calcined from 610 to 650 °C was analyzed by SEM and TEM; from these results, the typical morphology corresponds to nanostructured laminas. An increase in the inner porosity while increasing the calcination temperature was also observed. The gas sensing characterization was performed at 400 °C, revealing times of response of approximately 10 s in both oxygen and carbon dioxide. The resistance variations were 26 and 4 Ω, respectively. The ability of nanostructured GdCoO₃ to detect changes in the concentration of O₂ and CO₂ was studied. In CO₂, unique curves were obtained for each gas concentration; however, the results registered in O₂ revealed a lower performance.

© 2009 Elsevier B.V. All rights reserved.

1. Introduction

In recent years, the impact of the global warming on the climate change has been of particular concern worldwide [1–3]. As it is well known the global warming is caused by the emission of large amounts of carbon dioxide, methane and other greenhouse gases to the atmosphere. For the detection and monitoring of these gases, reliable solid-state sensor materials are of great importance. In this field, binary oxides such as SnO₂, ZnO and TiO₂ have been intensively studied. However, ternary and quaternary oxides, possessing a variety of crystal structures, are also of interest because of their notable gas sensing performance [4].

Particularly, Gd_{1-x}A_xCoO₃ (where A = alkali-earth metal), possessing the perovskite-type structure, has interesting properties and applications such as magnetotransport, thermoelectricity, mixed ionic–electronic conductivity for electrodes in solid oxide fuel cells, photocatalytic activity for the decomposition of dyes, phenols and substituted phenols, as well as gas sensors [5–9].

Moreover, although numerous studies can be found in the literature about the crystal structure, oxygen diffusion, electrical and electrochemical properties of LnMeO₃ (where Ln = rare earth and Me = transition metal), considerable less information is found about their gas sensing properties [10–13].

In a research made by Dutta et al. it was found that the perovskites LaMeO₃ (Me = Mn, Co, Ni, Fe) show a small sensitivity to oxygen. However, high sensitivity to C₃H₆ was observed in these compounds [14]. According to these authors, the sensitivity to C₃H₆ for lanthanum perovskites was increased in the following sequence: LaMnO₃ > LaCoO₃ ≫ LaNiO₃ > LaFeO₃ > PrCoO₃. This was explained by the high activity for oxygen reduction to oxide ion in LaCoO₃; however, in PrCoO₃ mainly the opposite behavior was observed (high activity for the oxidation reaction). Even though LaCoO₃ and PrCoO₃ are p-type semiconductors, the different electron transfer behaviors measured during their exposition to a hydrocarbon atmosphere is related to the larger amount of high-spin Co³⁺ in LaCoO₃. Moreover, for strontium-doped LaCoO₃ (La_{1-x}Sr_xCoO₃), the surface activity for oxygen reduction was increased by increasing the amount of strontium, which produced a larger amount of high-spin Co³⁺ [15]. Besides, the partial substitution of lanthanum by strontium produced an increase in the oxygen non-stoichiometry in La_{1-x}Sr_xCoO₃.

Recently, the electric and magnetic properties of GdCoO₃, Gd_{0.9}Sr_{0.1}CoO₃ and Gd_{0.9}Ba_{0.1}CoO₃, at low temperature, were studied by Ivanova et al. [16,17]. They identified the presence of Co³⁺, which below room temperature was in a fixed low-spin state. Since the extent of Co³⁺ in LaCoO₃ is strongly related to the detection of C₃H₆, the presence of Co³⁺ in GdCoO₃ suggests a gas response to reducing or electron donating gases such as CO₂. Therefore, in a first approach, the gas sensing properties of GdCoO₃ are worth to study in CO₂.

On the other hand, nanostructured materials, exhibiting extensive nanoporosity, are of special relevance in gas sensing and

* Corresponding author at: Departamento de Física CUCEI, Universidad de Guadalajara, Blvd. Marcelino García Barragán 1421, Sector Reforma, 44410 Guadalajara, Jalisco, Mexico. Tel.: +52 33 33 45 41 47; fax: +52 33 33 45 41 47.

E-mail address: michelucr@yahoo.es (C.R. Michel).

heterogeneous catalysis, because of their high surface to volume values. Therefore, a large number of chemical methods have been investigated to develop this kind of materials. One of the most simple and cost-effective routes to synthesize nanostructured and nanoporous materials is the solution-polymerization method. This method involves the use of a polymer precursor like polyvinyl alcohol (PVA) or polyethylene glycol (PEG), which promotes the homogeneous distribution of the ions throughout a polymer network. After the removal of organic matter by thermal decomposition, a nanostructured and nanoporous inorganic material is produced [18,19]. On the other hand, polyvinyl pyrrolidone (PVP), as well as PVA, have been successfully used for the preparation of metal nanoparticles and bimetallic nanoclusters [20–24]. In these syntheses, PVP and PVA act as polymer-type protective agents against oxidation and prevent nanoparticle agglomeration caused by electrostatic forces.

Since few is known about the gas sensing properties of an important class of inorganic oxides, like cobalt perovskites, in this work, the synthesis of GdCoO_3 by an aqueous solution-polymerization route using a combination of PVA and PVP was explored. The purpose of using these polymers was to avoid particle agglomeration in solution, and to obtain a nanostructured material. Due to carbon dioxide plays a key role in the global climate change, its detection and monitoring is of great relevance; therefore, the DC electrical characterization of GdCoO_3 thick films was investigated in a first approach in carbon dioxide, oxygen and air. Oxygen was chosen because it has the opposite behavior than carbon dioxide, in the sense that this gas can donate electrons instead of taken them from the material. The use of oxygen would give also information about the gas selectivity of GdCoO_3 . The air was used as a reference gas in order to reproduce the actual environment of the sensor.

2. Experimental

Polycrystalline GdCoO_3 was prepared by an aqueous solution-polymerization route: in a typical synthesis 3.16 g of $\text{Gd}(\text{NO}_3)_3 \cdot 6\text{H}_2\text{O}$ (Alfa Aesar) and 2.9 g of $\text{Co}(\text{NO}_3)_2 \cdot 6\text{H}_2\text{O}$ (J.T. Baker) were dissolved in 30 ml of deionized water. In another beaker, 0.22 g of PVA (Sigma) and 0.22 g of PVP (Sigma–Aldrich) were dissolved under strong stirring in hot deionized water (80 °C). Then, the solutions were mixed and stirred for 5 h without presence of precipitation. The evaporation of the resulting solution was made by microwave radiation producing a fluffy brown powder, which was pre-heated at 200 °C for 4 h. Further calcination was made from 500 to 650 °C in air, using a heating rate of 100 °C/h. The calcined powders were analyzed by X-ray powder diffraction (XRD) at room temperature, using a Rigaku Miniflex apparatus (Cu $\text{K}\alpha$ radiation). The morphology of the samples was observed by scanning electron microscopy (SEM), using a Jeol JSM 5400LV microscope. Transmission electron microscopy (TEM), using a Jeol JEM1010 microscope was used for nanoparticle characterization.

In order to test nanostructured GdCoO_3 as a gas sensor material, thick films were prepared by the screen printing technique. By this method, 0.1 g of the powder was placed into a plastic vial containing 1 ml ethyl alcohol absolute; then, the suspension was sonicated for 5 min. Circular thick films, with 5 mm of diameter, and thickness of 300 μm were formed after depositing the suspension inside a ceramic ring. Silver wires fixed to the ceramic disc were used as electrical contacts. Fig. 1 shows the scheme of the sensor device. Prior to the electrical characterization, the films were sintered at 600 °C for 2 h. The measurements were performed in DC by the two-point probe method, using a data acquisition system (Agilent 34970A) and a digital voltmeter (Agilent 34401A). The polarization curves were carried out using a Solartron 1285A potentiostat/galvanostat. The test gases used in this work were synthetic air, CO_2 and O_2 , which were supplied through a tubular furnace at a flow rate of 0.22 sccm. The gases were delivered by a multichannel mass flow controller, MKS Instruments 647C.

3. Results and discussion

3.1. X-ray powder diffraction

XRD was used to investigate the temperature of formation of GdCoO_3 ; with this purpose, the powders annealed at 200 °C were calcined from 500 to 650 °C; Fig. 2 shows the corresponding XRD patterns. The calcination at 500 °C produced an amorphous mate-

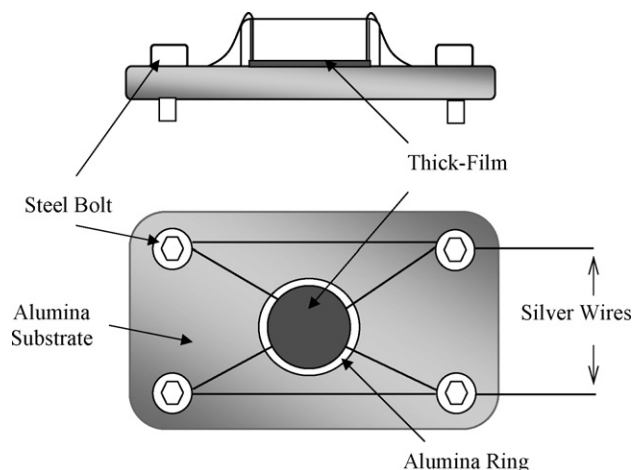


Fig. 1. Diagram of the sensor device used in the gas sensing characterization.

rial; however, at 600 °C an incipient formation of GdCoO_3 can be noticed by the presence of the main peak placed at $2\theta = 33.8^\circ$. The calcination from 610 to 640 °C produced an improvement in the crystallization of the powder; however, the presence of Gd_2O_3 and Co_3O_4 can be noticed in these patterns. Firing at 650 °C permitted the identification of the all the peaks of GdCoO_3 by using the JCPDF File No. 25-1057. Besides, a significant reduction of the secondary phases was achieved at this temperature. It is worth to mention that the JCPDF file corresponds to a GdCoO_3 sample obtained under high oxygen pressure.

The XRD pattern of the sample annealed at 650 °C was also compared with that reported by Mahata et al., for a GdCoO_3 sample calcined at 700 °C [9]. For the preparation of this perovskite, these authors employed a hydrothermal method, using gadolinium nitrate, cobalt acetate and pyridine-2,3-dicarboxylic acid as starting materials. Significant differences between these results were not observed. Besides, even though some authors report the prepa-

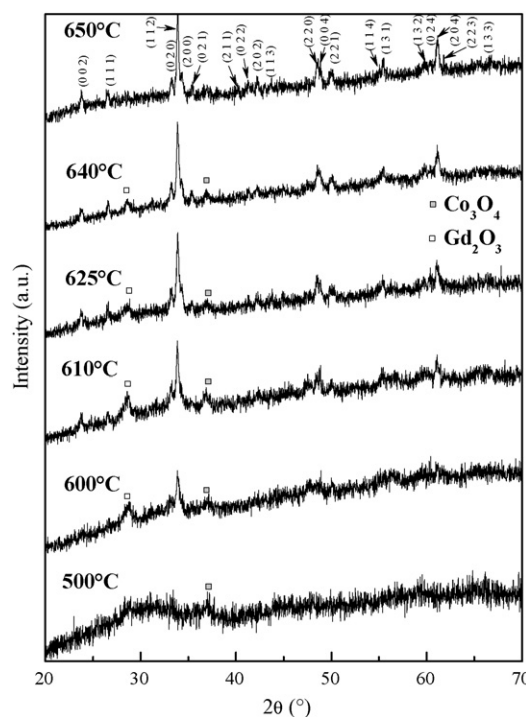


Fig. 2. XRD patterns of precursor powders of GdCoO_3 calcined from 500 to 650 °C in air.

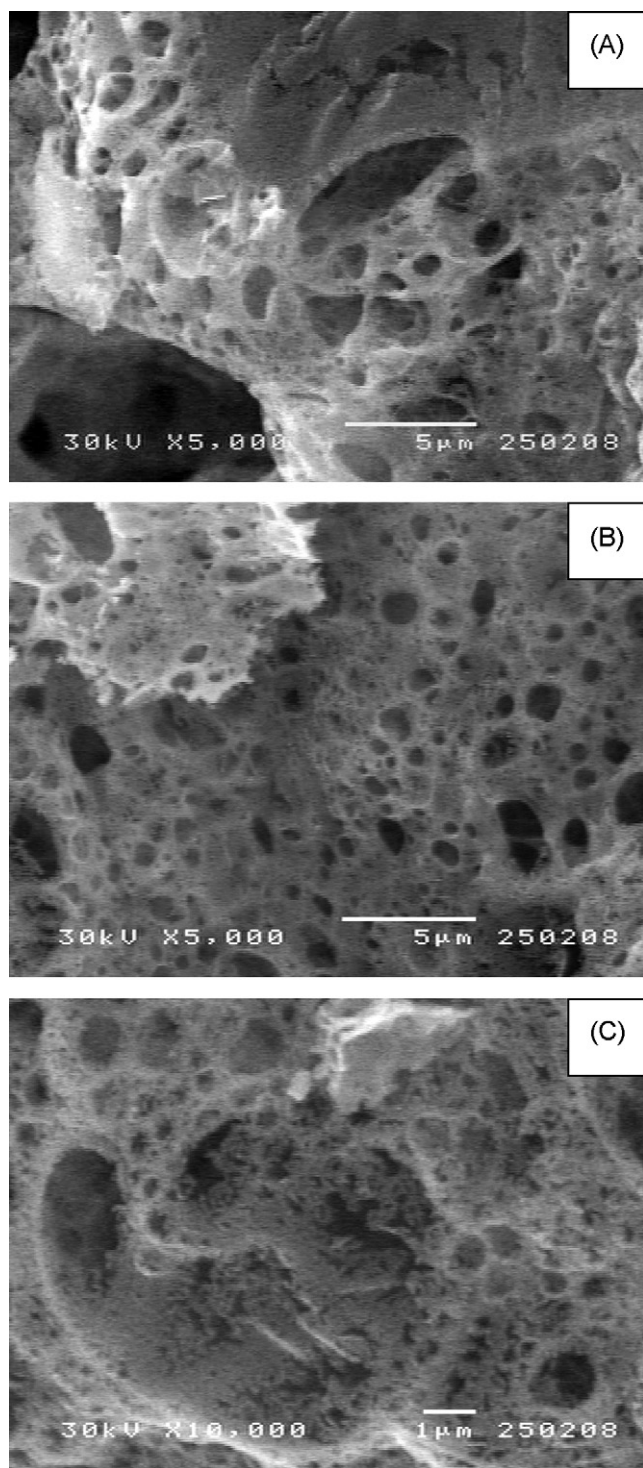


Fig. 3. SEM images of GdCoO_3 calcined at: (A) 600 °C, (B) 625 °C and (C) 650 °C.

ration GdCoO_3 , they do not provide XRD results, or these contain a mixture of crystalline phases, preventing their comparison with the present results [25,26]. In summary, the solution-polymerization method provides a cost-effective and simple alternative route to obtain GdCoO_3 , at a relative low temperature.

3.2. Electron microscopy

The surface morphology of samples fired at 600, 625 and 650 °C was observed by SEM. Fig. 3(A–C) shows typical images of these

powders, respectively. From these results, an extensive porosity can be observed in the three samples; however, a significant change in the microstructure cannot be established. The pores of these powders are attributed to the gases released during the thermal decomposition of organic matter, which are mainly CO_2 , water vapor and NO_x .

The formation of nanoparticles and nanopores was identified by TEM, Fig. 4(A–C) shows images of the samples fired at 600, 625 and 650 °C, respectively. The morphology of the powder produced at 600 °C (Fig. 4A) corresponds to nanostructured laminas, which are formed by a compact network of nanoparticles of irregular shape. The average particle size, measured from several images, was 12 nm; its particle size distribution histogram is shown in Fig. 5A. When the annealing was made at 625 °C, porosity was developed as a consequence of nanoparticle coalescence (Fig. 4B); the average particle size was 21 nm, with the particle size distribution shown in Fig. 5B. In this case a bimodal size distribution can be observed due to the formation of larger particles. On the other hand, the calcination at 650 °C mainly produced a continuous phase, which made difficult the determination of the size of individual particles. However, the microstructure of this powder suggests the easier transport of charge carriers, due to a smaller amount of grain boundaries was identified.

3.3. Electrical and gas sensing characterization

Due to the powder calcined at 650 °C had the lowest amount of secondary phases, as well as the larger pores, the electrical and gas sensing characterization was carried out on this material. Fig. 6 shows the variation of electrical conductivity with T^{-1} (Arrhenius-type plots) recorded in dry air, CO_2 and O_2 . Clearly, a semiconductor behavior can be noticed in these graphs. In CO_2 a quasi-linear trend can be observed; the calculated activation energy for the mobility of charge carriers (E_A) was 0.47 eV. On the other hand, in dry air and oxygen is possible to identify two branches, with a metal-to-semiconductor transition temperature placed at ~ 280 °C. Below this temperature, E_A was 0.38 eV; whereas above 280 °C, E_A was 0.49 eV.

The plots of σ vs. T^{-1} obtained in this work were compared with those reported by Thornton et al., and Takeda et al. for the same perovskite [25,26]. Significant differences in the preparation of GdCoO_3 must be mentioned. For instance, Thornton et al. reported a synthesis method based in the thermal decomposition of gadolinium chloride and potassium cobalticyanide. Further calcination in air was made by these authors at 927 °C. On the other hand, Takeda et al. used the solid-state reaction method with Gd_2O_3 and Co_3O_4 as starting materials. As it is the usual in this method, the reagents were mixed, pressed into pellets, and fired at high temperature (1200 °C). Although, different methods to synthesize GdCoO_3 were used, the resulting Arrhenius-type graphs show similar general characteristics compared to those shown in Fig. 6. These graphs also display metal-to-semiconductor transition temperatures around 290 °C. The small differences may be attributed to factors such as sample microstructure and oxygen vacancy concentration, among others.

Also from Fig. 6, the conductivity measured in oxygen was the largest in the entire temperature range. However, in carbon dioxide the smallest values were recorded. The explanation of these results will be provided later in this paper, on the basis of changes in the amount of charge carriers, when GdCoO_3 is in contact with an oxidizing or an electron donating gas.

On the other hand, in order to evaluate the dynamic response of resistance of GdCoO_3 thick films, dry air was supplied at 0.22 sccm for about 10 min, until a stable resistance was registered. Then, CO_2 or O_2 with the same gas flow rate was delivered for 1 min. During this time the air was shut off. Fig. 7 shows typical graphs recorded

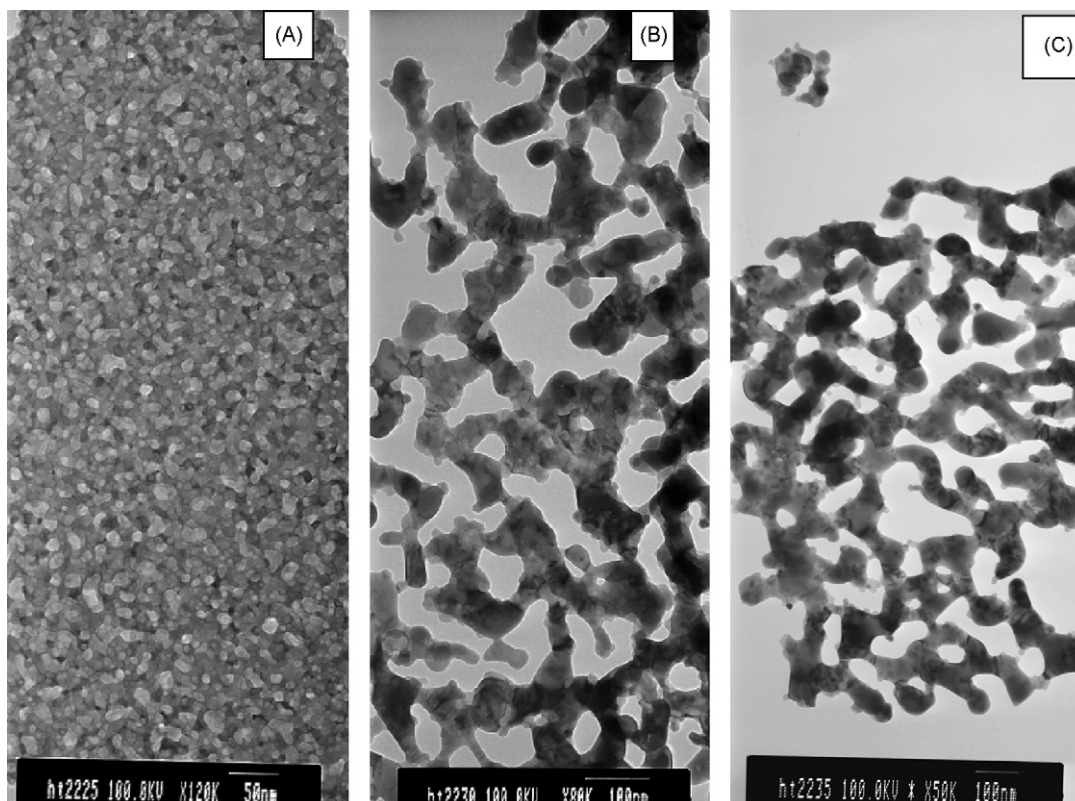


Fig. 4. TEM photos of GdCoO₃ fired at: (A) 600 °C, (B) 625 °C and (C) 650 °C.

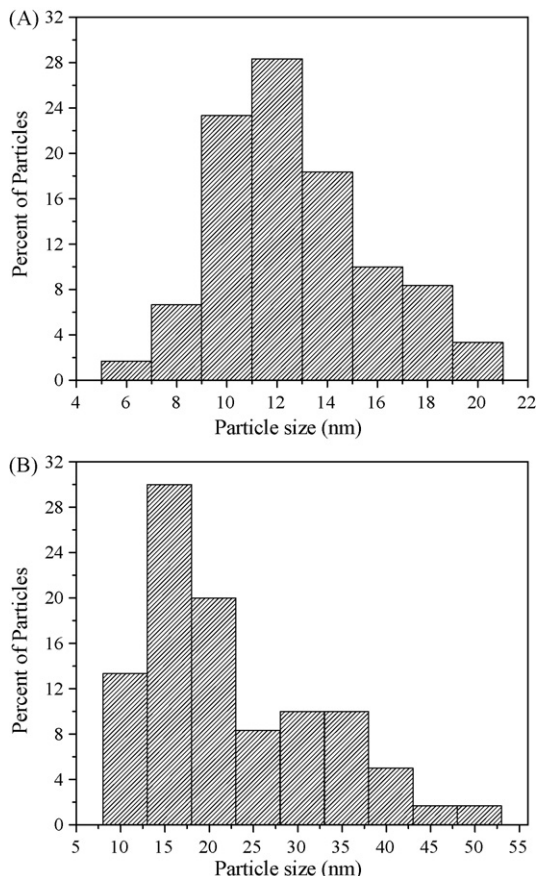


Fig. 5. Particle size distributions of GdCoO₃ calcined at: (A) 600 °C and (B) 625 °C.

in CO₂ (A) and O₂ (B) at 400 °C; at this temperature, the most satisfactory results were obtained in both gases. In CO₂, an average increase of resistance of 26 Ω was systematically registered, whereas in O₂, an average variation of approximately −4 Ω was obtained. The smaller variation of the resistant in O₂ can be associated to a smaller variation in the concentration of this gas, since synthetic air contains 21% of oxygen. About the times of response, in CO₂, the 50% of the full resistance variation occurs in ~10 s. In O₂, the 90% of the total variation takes place in ~10 s, indicating a faster response to oxygen. Moreover, upon the shift to air, the time to recover the 80% of the initial resistance was 7.8 s in oxygen; whereas in carbon dioxide was 5.3 s.

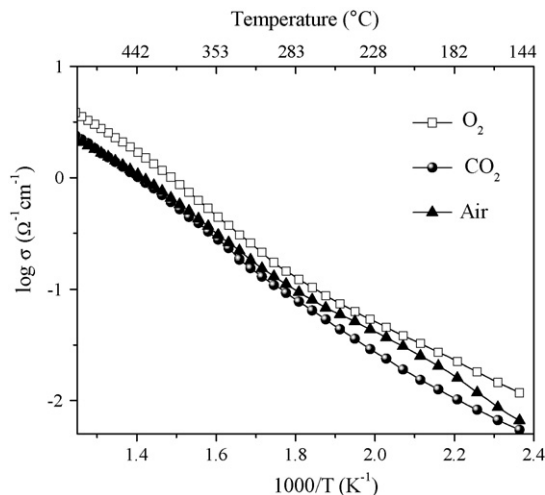


Fig. 6. Arrhenius plots for GdCoO₃ thick films measured in air, O₂ and CO₂.

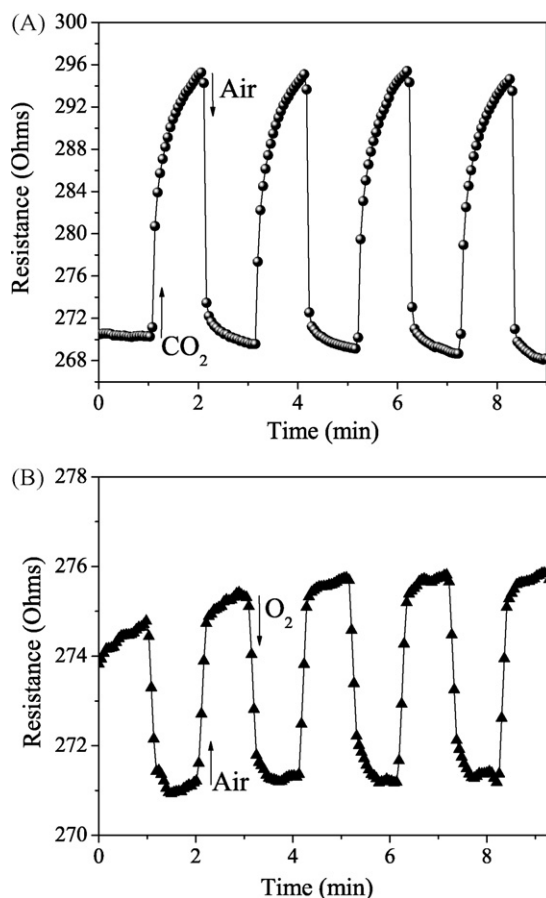


Fig. 7. Dynamic response of resistance plots for GdCoO₃ thick films in (A) CO₂ and (B) O₂ (400 °C).

In order to test the ability of GdCoO₃ to detect variations in the type of gas, air, CO₂ and O₂ were alternatively introduced; Fig. 8 shows a typical graph recorded at 400 °C. Clearly, a distinctive resistance behavior is displayed for each gas type, along with a full recovery of the original resistance after each gas dose. After the introduction of carbon dioxide an increase of resistance of 24 Ω was measured; whereas in oxygen, the decrease was 4 Ω. These results are in agreement with those shown in Fig. 7, revealing a confident response of GdCoO₃ to the detection of these gases.

On the other hand, according to Moseley et al., GdCoO₃ is a p-type semiconductor material because its resistance decreases in

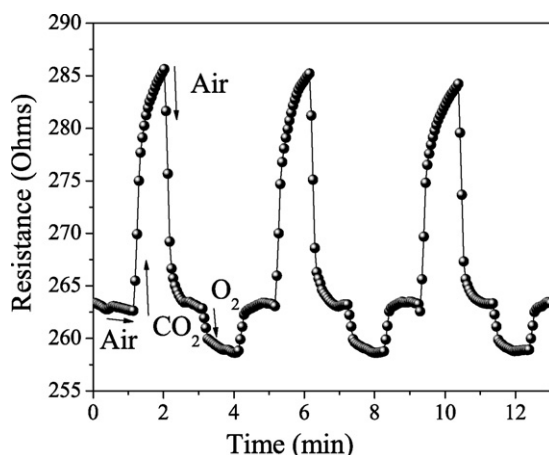


Fig. 8. Gas response of a GdCoO₃ thick film in air, CO₂ and O₂.

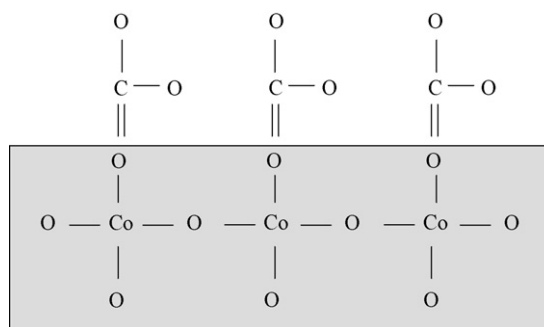
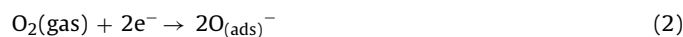


Fig. 9. Scheme of the CO₂ adsorption in GdCoO₃.

presence of oxygen, whereas in carbon dioxide occur the opposite behavior [4]. The mechanism of oxygen sensing in oxide semiconductors has been studied time ago by several authors. This is based on changes in electrical resistance (or conductance), caused by the electron transfer during chemisorption [27]. Specifically, the oxygen adsorbed at the surface of the oxide removes electrons producing a depletion layer, which increase the number of holes. Then, since holes are the charge carriers, the conductance is increased.

The mechanism of oxygen adsorption is highly dependent on the temperature, and may occur by one of the following reactions:



where suffix (ads) means the adsorbed species.

On the other hand, the mechanism of detection of CO₂ can be explained in terms of the adsorption of this gas on the surface of a material. This phenomenon has been greatly studied in zirconia, and in some rare earth and alkali-earth metal oxides [28–32]. Several techniques such as temperature-programmed desorption (TPD), microcalorimetry and Fourier transform infrared spectroscopy (FTIR) have been used for this purpose. In the case of zirconia, Bachiller-Baeza et al., found that different surface species such as bicarbonate, monodentate, and bidentate carbonates were formed upon the adsorption of CO₂, involving acid–base pair sites: Zr⁴⁺–O²⁻ [30]. These authors also found that the formation of a specific kind of carbon compound depends on the crystal structure of the zirconia.

The adsorption of CO₂ in complex oxides has been less studied in our knowledge. According to Ishihara et al., the formation of a thin carbonation layer on the surface of CuO–BaTiO₃ and CuO–SrTiO₃ sensors can be involved in the detection of this gas [33]. However, for other oxide perovskites little information is available about this topic.

From Fig. 7A, the contact of GdCoO₃ with CO₂ produced a decrease in the number of charge carriers, increasing its resistance. This suggests that electrons from CO₂ molecules combine with holes of the conduction band of the perovskite, reducing the conductivity. A possible mechanism involved in this process may be:



Fig. 9 shows a simplified scheme of the suggested CO₂ adsorption mechanism in GdCoO₃. The lower shadow portion of this figure represents planes containing cobalt and oxygen ions of the perovskite, where the oxygen ions occupy octahedral sites. Since gadolinium ions occupy the center positions of the unit cell, these were not included in this view, and their activity in CO₂ adsorption may be considerably smaller.

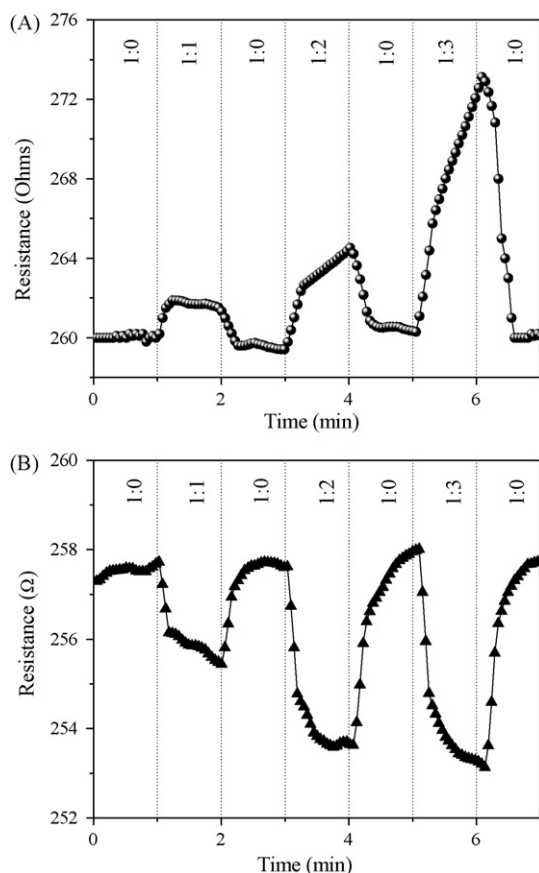


Fig. 10. Variation of resistance measured using different air:CO₂ and air:O₂ gas ratios.

With the purpose of investigating a quantitative response produced by a change in the gas concentration, the variation of resistance with time was measured in several mixtures of air and carbon dioxide (air:CO₂), and air and oxygen (air:O₂). In these experiments multiples of 0.22 sccm gas flows were supplied at 400 °C. Fig. 10 shows the corresponding graphs obtained in carbon dioxide (A) and oxygen (B). From these results is clear that increasing the concentration of the test gases, a proportional variation of the resistance was measured. These results are consistent with those shown in Fig. 7, because the combination of the test gas with air implies a reduction of the total resistance change.

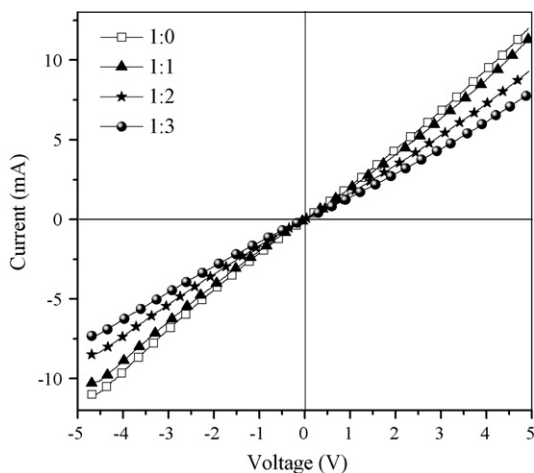


Fig. 11. Polarization curves of GdCoO₃ obtained using mixtures of air and CO₂ (air:CO₂), measured at 400 °C.

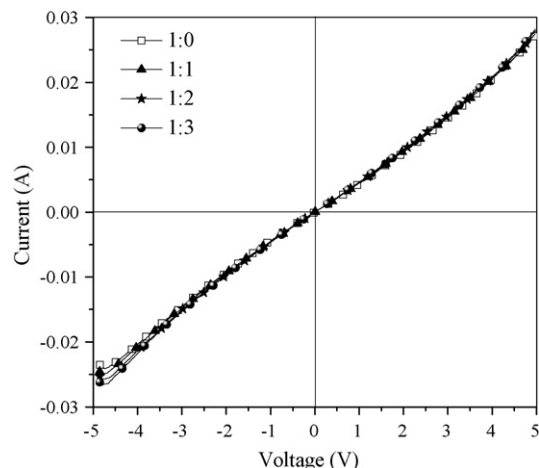


Fig. 12. *I*-*V* curves of GdCoO₃ measured using several air:O₂ gas flow ratios at 400 °C.

The measurement of the polarization response was another characterization technique to test the detection of GdCoO₃ to different gas concentrations. The *I*-*V* curves were registered from -5 to 5 V, using the same air:CO₂ and air:O₂ mixtures than before, Figs. 11 and 12 show the corresponding results (400 °C). In CO₂, Fig. 11 shows that an increase in the CO₂ concentration from 1:0 to 1:3 produced an increase in current from 7.8 to 12 mA. Well defined curves for each CO₂ concentration can be observed. In the figure, at negative voltages, the opposite behavior was obtained as expected; with current values slightly smaller in magnitude. Moreover, a nearly linear behavior can be observed in each curve, at both positive and negative voltages.

Fig. 12 shows the polarization curves recorded in oxygen. Even though, larger current values were obtained in this gas, compared with those registered in CO₂, a clear overlapping of the four curves is observed. This overlapping is more evident when positive voltages were applied. These results are consistent with those obtained in dynamic response (Fig. 7B), because a reduction of resistance of GdCoO₃ in oxygen causes an increase in the current. Moreover, the graphs of Fig. 12 indicate that if air is used as the reference gas, GdCoO₃ will have a lower performance.

4. Conclusions

In this work, GdCoO₃ was prepared by an aqueous solution-polymerization method using a combination of PVA and PVP. The use of these inexpensive polymer precursors resulted in an effective method to obtain nanostructured GdCoO₃. The calcination of precursor powders from 610 to 650 °C permitted to control the particle size and porosity. The annealing at 650 °C produced GdCoO₃ powder.

From the results of the gas sensing characterization is possible to conclude that although the variation of resistance in CO₂ and O₂ were not as large as other materials, very reproducible patterns can be obtained. Evidently the performance in carbon dioxide is better than in oxygen; even though the carbon dioxide is considered as a stable molecule. Besides, the dynamic response of resistance tests performed in different gas mixtures, were used to demonstrate that nanostructured GdCoO₃ can detect variations in gas concentration. The polarization graphs display well differentiable curves for each gas mixture, except in oxygen at positive voltages. From these results GdCoO₃ can be considered as a suitable carbon dioxide gas sensor material.

Acknowledgements

Financial support from the Coordinación General Académica of the Universidad de Guadalajara, the National Council of Science and Technology of Mexico (CONACYT) under Grant I-52204, and COECYTJAL (Grant PS-2008-847) is greatly acknowledged. AHM and JPML are grateful to CONACYT for their graduate scholarships.

References

- [1] P. Cox, C. Jones, *Science* 321 (2008) 1642.
- [2] M. Parry, O. Canziani, J. Palutikof, *World Meteorol. Org. Bull.* 57 (2008) 1.
- [3] J. Ahn, E.J. Brook, *Science* 322 (2008) 83.
- [4] P.T. Moseley, A.M. Stoneham, D.E. Williams, in: P.T. Moseley, J. Norris, D.E. Williams (Eds.), *Techniques and Mechanisms in Gas Sensing*, Adam Hilger, Bristol, 1991, pp. 122–127.
- [5] C. Rey-Cabezudo, M. Sánchez-Andújar, J. Mira, A. Fondado, J. Rivas, M.A. Señaris-Rodríguez, *Chem. Mater.* 14 (2002) 493.
- [6] J.W. Moon, W.S. Seo, H. Okabe, T. Okawa, K. Koumoto, *J. Mater. Chem.* 10 (2000) 2007.
- [7] Y. Takeda, H. Ueno, N. Imanishi, O. Yamamoto, N. Sammes, M.B. Phillips, *Solid State Ionics* 86–88 (1996) 1187.
- [8] H.D. Wienhöfer, H.G. Bremes, U. Nigge, *Solid State Ionics* 175 (2004) 93.
- [9] P. Mahata, T. Aarti, G. Madras, S. Natarajan, *J. Phys. Chem. C* 111 (2007) 1665.
- [10] C.N.R. Rao, B. Raveau, *Transition Metal Oxides*, VCH, New York, 1995.
- [11] N.Q. Minh, T. Takahashi, *Science and Technology of Ceramic Fuel Cells*, Elsevier, Amsterdam, 1995.
- [12] S. Trasatti, G. Lodi, in: S. Trasatti (Ed.), *Electrodes of Conductive Metallic Oxides*, Elsevier, Amsterdam, 1981, pp. 521–626.
- [13] C.R. Michel, E. López-Mena, A.H. Martínez, *Talanta* 74 (2007) 235.
- [14] A. Dutta, T. Ishihara, H. Nishiguchi, Y. Takita, *J. Electrochem. Soc.* 151 (2004) H122.
- [15] T. Horita, K. Yamaji, N. Sakai, H. Yokokawa, A. Weber, E. Ivers-Tiffée, *J. Electrochem. Soc.* 148 (2001) A456.
- [16] N.B. Ivanova, N.V. Kazak, C.R. Michel, A.D. Balaev, S.G. Ovchinnikov, A.D. Vasil'ev, N.V. Bulina, E.B. Panchenko, *Phys. Solid State* 49 (2007) 1498.
- [17] N.B. Ivanova, N.V. Kazak, C.R. Michel, A.D. Balaev, S.G. Ovchinnikov, *Phys. Solid State* 49 (2007) 2027.
- [18] C.R. Michel, E. López-Mena, A.H. Martínez-Preciado, *Mater. Sci. Eng. B* 141 (2007) 1.
- [19] M.A. Gülgün, M.H. Nguyen, W.M. Kriven, *J. Am. Ceram. Soc.* 82 (1999) 556.
- [20] P. Lu, J. Dong, N. Toshima, *Langmuir* 15 (1999) 7980.
- [21] T. Teranishi, M. Miyake, *Chem. Mater.* 11 (1999) 3414.
- [22] D. Li, S. Komarneni, *J. Am. Ceram. Soc.* 89 (2006) 1510.
- [23] C.C. Yang, C.C. Wan, Y.Y. Wang, *J. Electrochem. Soc.* 153 (2006) J27.
- [24] Y.H. Rho, K. Kanamura, *J. Electrochem. Soc.* 151 (2004) A1406.
- [25] G. Thornton, F.C. Morrison, S. Partington, B.C. Tofield, D.E. Williams, *J. Phys. C* 21 (1988) 2871.
- [26] Y. Takeda, H. Ueno, N. Imanishi, O. Yamamoto, N. Sammes, M.B. Phillips, *Solid State Ionics* 86 (1996) 1187.
- [27] K.W. Kolasinski, *Surface Science*, Wiley, Chichester, 2008.
- [28] W. Hertl, *Langmuir* 5 (1989) 96.
- [29] K. Pokrovski, K.T. Jung, A.T. Bell, *Langmuir* 17 (2001) 4303.
- [30] B. Bachiller-Baeza, I. Rodríguez-Ramos, A. Guerrero-Ruiz, *Langmuir* 14 (1998) 3556.
- [31] H. Tsuji, A. Okamura-Yoshida, T. Shishido, H. Hattori, *Langmuir* 19 (2003) 8793.
- [32] X.P. Wang, J.J. Yu, J. Cheng, Z.P. Hao, Z.P. Xu, *Environ. Sci. Technol.* 42 (2008) 614.
- [33] T. Ishihara, K. Kometani, Y. Mizuhara, Y. Takita, *J. Electrochem. Soc.* 139 (1992) 2881.